Phase separation and thermally induced metal-insulator transition in heavily doped silicon (Si:B)

1998 J. Phys.: Condens. Matter 10 2963

(http://iopscience.iop.org/0953-8984/10/13/013)

J. Phys.: Condens. Matter **10** (1998) 2963–2971. Printed in the UK PII: S0953-8984(98)90773-1

Phase separation and thermally induced metal–insulator transition in heavily doped silicon (Si:B)

K H Kim, J P Wang, W C H Joiner and Y H Kim

Department of Physics, University of Cincinnati, Cincinnati, OH 45221-0011, USA

Received 13 January 1998

Abstract. A thermally induced genuine metal–insulator transition is observed through detailed far-infrared studies of a heavily boron-doped silicon with boron concentration slightly below the metal–insulator transition. We found that a phase separation instability plays an important role in the metal–insulator transition and Drude and diffuse metallic (Anderson metallic) phases coexist for temperatures above 110 K. Below 110 K, the disorder-induced Anderson insulator phase emerges within the metallic host, and its volume fraction reaches 0.4 at 10 K.

A random potential introduced into an ideal metallic system leads to the localization of electronic states up to a critical energy (E_c), called the mobility edge, which separates extended states from localized states [1]. Alternatively, in a semiconductor the phase transition from the insulating to the metallic state can also be induced by adding impurity dopant atoms to the host, although it is still a debatable issue how and what kind of metallic state is formed in heavily doped semiconductors. In either case when the Fermi energy, $E_F < E_c$, the system exhibits insulating behaviour even though the density of states at E_F remains finite.

It is generally accepted that the heavily doped semiconductor is regarded as a model random system best described by Anderson's Fermi glass model of non-interacting localized electrons. However, there is increasing evidence that the long-range Coulomb interaction between localized electrons becomes dominant in the insulating phase of the heavily doped semiconductor when the carrier hopping is sufficiently suppressed at low temperatures [1]. As a result a parabolic soft gap is opened at E_F in the single-particle density of states and the subsequent temperature dependence of the carrier transport is fundamentally changed from that of the Mott variable-range hopping, as reported in the detailed transport studies of heavily doped semiconductors [2, 3].

In an attempt to look into the nature of the metal–insulator transition and Coulomb interactions, we carried out far-infrared reflectivity and magnetic susceptibility measurements of boron-doped silicon (Si:B) with carrier density (n) slightly below the critical carrier density (n_c). With this carrier density, we are able to pass through the metal–insulator transition by thermal tuning of the highest occupied energy level across E_c. Since the infrared dynamics of localized carriers is expected to be markedly different from that of the metallic phase [4], far-infrared studies of heavily doped silicon, together with transport and magnetic susceptibility measurements, are expected to yield critical information to characterize the carrier dynamics in the vicinity of the metal–insulator transition.

0953-8984/98/132963+09$19.50

In this work, we obtained Drude-like normal metallic behaviour above 250 K. As the temperature decreases below 250 K, we found that phase separation of the charge carriers occurs, and causes changes in the transport and far-infrared properties. Thus a nearly insulating diffuse (Anderson) metallic phase begins to emerge with its volume fraction, f_m, reaching unity at $\approx$110 K. This is demonstrated by a decrease in the dc conductivity, and corresponding changes in the infrared conductivity, as the temperature is lowered to 110 K, but a temperature-independent Pauli-like susceptibility throughout this temperature range. We found that the dc conductivity of the Anderson metallic phase $\sigma_m(\omega = 0, T)$ shows a power law behaviour, $\sigma_m(0, T) = \sigma_0 + bT^\gamma$ with $\gamma \approx 1.5 \pm 0.5$, $b \approx 0.01$ and $\sigma_0 \approx 16.8\ \Omega^{-1}\ \mathrm{cm}^{-1}$. As the system is further cooled below 110 K, the insulating phase starts to appear within the Anderson metallic host with a volume fraction which monotonically increases with decreasing temperature, approaching 0.4 at 10 K. The corresponding susceptibility of the insulating phase can be fitted to the form $\chi \propto (T+13)^{-1}$, suggesting antiferromagnetic interaction between neighbouring localized carriers.

Commercially available Si:B single crystal wafers (500 μm thick) grown along the $\langle 111 \rangle$ direction were used. The carrier density, n, was estimated from the dc conductivity and the low-magnetic-field Hall measurements at room temperature. The Hall measurement yielded $n \approx 2.8 \times 10^{18}\ \mathrm{cm}^{-3}$ while the dc conductivity gave $n \approx 3.6 \times 10^{18}\ \mathrm{cm}^{-3}$, ensuring that $n < n_c \approx 4.0 \times 10^{18}\ \mathrm{cm}^{-3}$ [5]. The discrepancy between the dc and Hall measurements is not uncommon [6].

The temperature dependence of σ_{dc} was measured using the van der Pauw method [7]. Electrical contacts were made using the indium spot diffusion technique. Typical contact resistance was less than 2 Ω at 4.2 K and the ohmic behaviour of the contacts was checked with different excitation currents. The sample temperature was controlled using a continuous-flow liquid helium cryostat for temperatures between 4.2 K and 350 K. A Quantum Design magnetometer was used to measure the magnetic susceptibility (χ) as a function of temperature. The infrared reflectivity was measured using a Fourier transform spectrometer (Bruker IFS 113V) for frequencies ranging from 20 cm^{-1} (2.5 meV) to 5000 cm^{-1} (620 meV). The complex dielectric function, $\varepsilon(\omega) = \varepsilon_1 + 4\pi\, \mathrm{i}\sigma_1/\omega$ was calculated from the reflectivity data using a Kramers–Kronig analysis.

Figure 1 shows dc conductivity, σ_{dc}, of Si:B for temperatures between 10 K and 350 K. Upon lowering the temperature from 350 K, σ_{dc} increases and reaches its maximum at $\approx$ 230 K, flattens out below 230 K and then starts to decrease at 200 K. However, below 60 K σ_{dc} decreases more slowly and appears to approach a finite value. The increasing σ_{dc} with decreasing temperature indicates that the system is in a genuine metallic state where the carrier relaxation mechanism is dominated by the scattering with phonons. We notice that the deviation from the metallic behaviour at around 230 K with σ_{dc} decreasing at lower temperatures is a signature of electron localization which arises from the scattering of electrons with the randomly distributed dopant ions. This scattering causes quantum interference of the electron wavefunction and this effect is more pronounced as the temperature decreases because the relevant dephasing inelastic length scale increases with decreasing temperature [8]. Therefore, the localization behaviour is progressively more evident as the temperature decreases. The physical origin of the levelling off in σ_{dc} below 60 K is not obvious from the transport data alone. However, it becomes clear in the analysis of far-infrared conductivity shown in figure 4.

Also shown in figure 1 is the carrier magnetic susceptibility, χ_c, measured between 4.2 K and 300 K. χ_c is obtained by subtracting the diamagnetic susceptibility of the silicon background. Hence, the data reflect the contribution of holes generated by doping. The approximately temperature-independent χ_c between 100 K and 300 K indicates that the

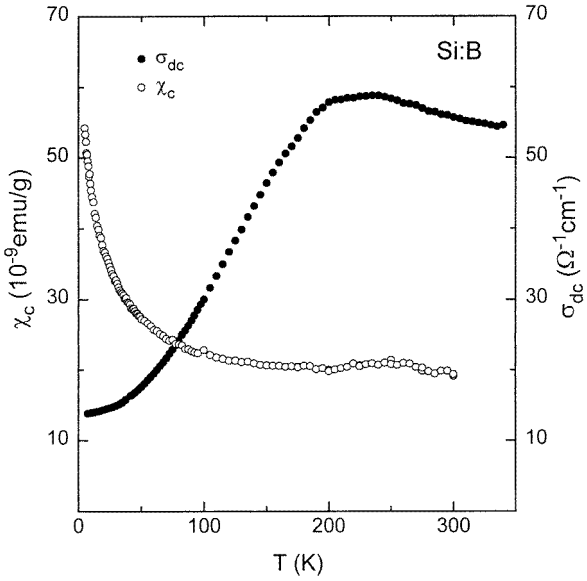

Figure 1. Temperature dependence of the dc conductivity and magnetic susceptibility of Si:B with a carrier concentration, $n = 3.6 \times 10^{18}$ cm^{-3} $< n_c$. The background magnetic susceptibility of silicon has been subtracted.

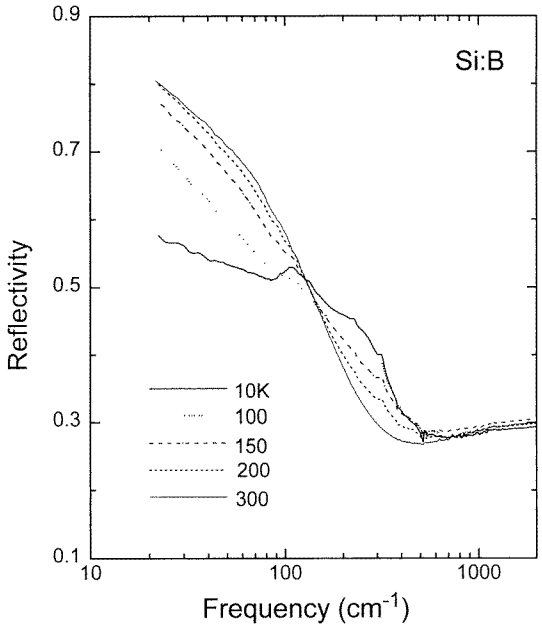

Figure 2. Far-infrared and infrared reflectivity data of Si:B at various temperatures.

system is still in the metallic regime even though σ_{dc} decreases with temperature. For temperatures below 100 K, χ_c starts to increase rapidly with decreasing temperature due to the emergence of the localized carriers. The onset of the increase of χ coincides with the levelling off of σ_{dc} below 100 K.

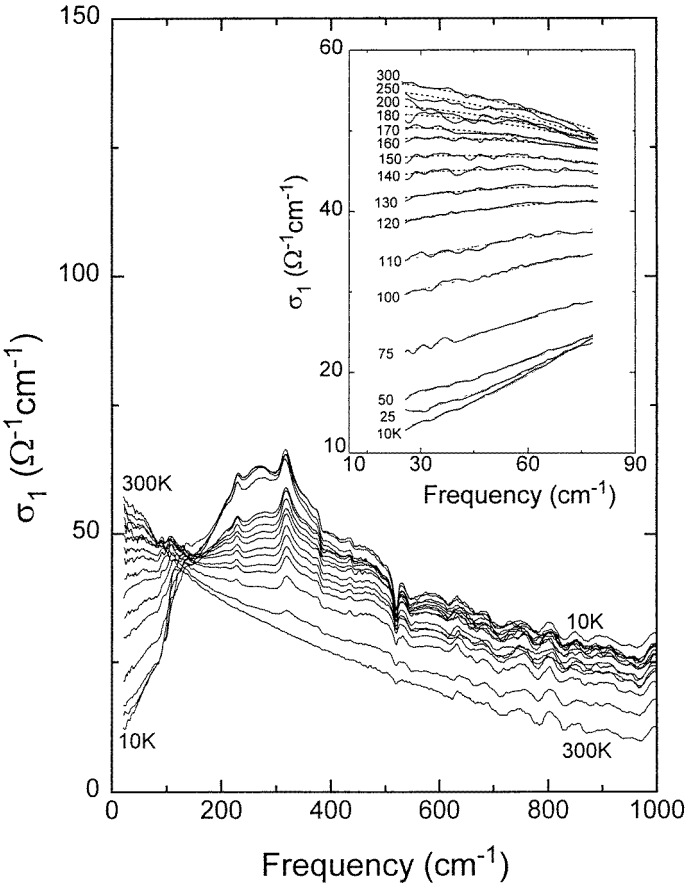

Figure 3. Real part of the far-infrared and infrared conductivities of Si:B at various temperatures. Inset: far-infrared tail of the conductivity fitted with appropriate fitting functions for the temperature range from 10 K to 300 K (see the text).

The infrared reflectivity of Si:B at various temperatures is displayed in figure 2, and shows remarkable changes with temperature. At 300 K, a typical Drude-like metallic response was found; the reflectivity approaches unity in the zero-frequency limit and shows the reflectivity minimum at ≈400 cm^{-1} resulting from the plasma behaviour of carriers. As the temperature is lowered below 300 K, the overall reflectivity systematically changes its behaviour; the reflectivity above 100 cm^{-1} increases while the reflectivity below 100 cm^{-1} decreases as the temperature decreases. This picture shows systematic oscillator strength transfer from the free carriers to the localized carriers as the temperature is lowered.

The real part of the frequency-dependent conductivity, $\sigma_1(\omega)$, calculated from the reflectivity data via the Kramers–Kronig transformation, is shown in figure 3 for frequencies between 2 cm^{-1} and 1000 cm^{-1}. A dramatic change from the Drude-like metallic behaviour to an insulating behaviour is readily seen upon lowering the sample temperature; the free carrier oscillator strength is transferred to the conductivity above ≈130 cm^{-1} which is identified as the crossover frequency, ω_c, above which the system does not distinguish whether the system is in the metallic or insulating state. Note that the crossover frequency

given by $\omega_c \sim \{(n_c - n)/n_c\}^{3\nu}$ (ν = critical exponent) [9], is independent of temperature, implying that the carrier concentration of the insulating phase remains constant. Also, weak absorption features develop at $\approx$125 cm^{-1}, $\approx$250 cm^{-1} and $\approx$325 cm^{-1} on top of the broad background at low temperatures. These weak features may be attributed to the valley–orbit splitting and 1s to 2p transitions of the hydrogen-like states of holes bound to dopant ions [10]. However, less than 1% of the total carriers go into the hydrogen-like impurity states at low temperatures as the sum rule indicates. This implies that the predominant contribution to $\sigma_1(\omega)$ comes from the carriers in the localized states induced by the random potential.

Details of data fitting of the low-frequency tail of $\sigma_1(\omega)$ are shown in the inset of figure 3. A satisfactory fit was obtained with the Drude conductivity,

$$\sigma_D(\omega, T) = \sigma_{dc}/[1 + (\omega\tau)^2] \tag{1}$$

for temperatures above 250 K and $\omega < \omega_c$ with the fitting parameter $\tau^{-1} \approx 140 + 0.19T$ cm^{-1}. However, our attempt to fit the data using $\sigma_D(\omega, T)$ alone failed for the data below 250 K. Instead the following linear combination

$$\sigma_1(\omega) = f_m(T)\sigma_m(\omega, T) + \{1 - f_m(T)\}\sigma_D(\omega, T) \tag{2}$$

gave the best result where

$$\sigma_m(\omega, T) = \sigma_m(0, T) + C_m\omega^{1/2} \tag{3}$$

which is the conductivity of the metallic side of the metal–insulator transition derived from the self-consistent calculation of Anderson localization based on the scaling theory [11]. $\sigma_m(0, T = 0)$ is the minimum metallic conductivity of the Anderson metallic phase and C_m is a constant. Thus, the corresponding expression for $\sigma_{dc}(T)$ becomes

$$\sigma_{dc}(T) = f_m(T)\sigma_m(0, T) + \{1 - f_m(T)\}ne^2\tau(T)/m^*. \tag{4}$$

Using the expression we found above for $\tau(T)$, and using the fact that $\sigma_{dc}(T) \approx ne^2\tau(T)/m^*$ for temperatures above 250 K, we find $m^* \approx 0.5m_e$, where m_e is the free electron mass, which is a reasonable value for silicon [12].

As we cool down the sample below 110 K, the fitting scheme used for temperatures above 110 K is no longer valid. Rather, an excellent fit was achieved using

$$\sigma_1(\omega) = \{1 - f_m(T)\}\sigma_i(\omega, T) + f_m(T)\sigma_m(\omega, T) \tag{5}$$

where

$$\sigma_i(\omega, T) = \sigma_i(0, T) + C_i\omega^2 \tag{6}$$

which is the conductivity for the insulating side of the metal–insulator transition also derived from the self-consistent calculation of Anderson localization for $\omega < \omega_c$ [11]. This suggests that the insulating phase starts to appear as the temperature decreases below 110 K. In this expression $\sigma_i(0, T)$ is the dc conductivity of localized carriers and C_i is a constant, related to C_m through the calculated expression $C_i/C_m = \pi^3/4\omega_c^{3/2} \approx 0.0053$ cm$^{3/2}$ with $\omega_c \approx 130$ cm^{-1} [11]. Therefore the volume fraction of the Anderson metallic phase, $\sigma_m(0, T)$, can be found from equations (2) and (4) or (5) and (6) using experimentally measured values of $\sigma_{dc}(T)$ and $\sigma_1(\omega, T)$, and assuming $f_m(T) = 1$ at 110 K as shown in figure 4. This latter assumption is justified because at 110 K $\sigma_1(\omega, T)$ can be fitted using equation (3) alone.

From (5) at $\omega = 0$, we find that both the Anderson metallic phase and the insulating phase contribute to the dc conductivity below 110 K:

$$\sigma_{dc} = (1 - f_m)\sigma_i(0, T) + f_m\sigma_m(0, T). \tag{7}$$

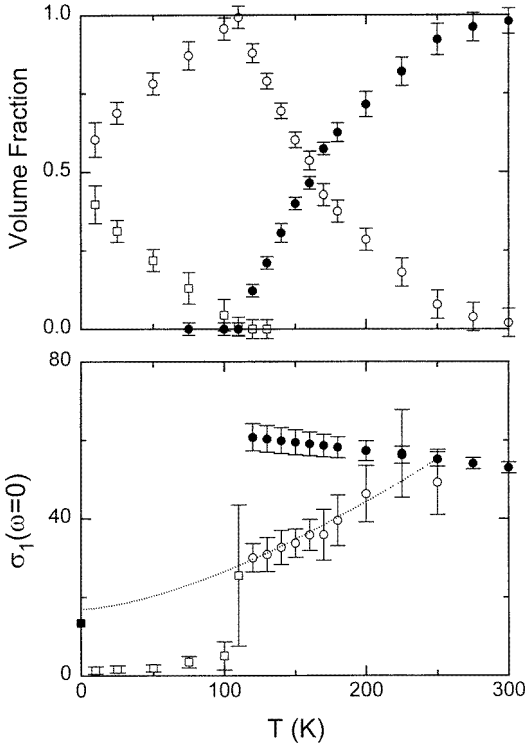

Figure 4. Upper panel: calculated volume fraction of each phase as a function of temperature (closed circle: Drude metallic phase; open circle: Anderson metallic phase; closed square: insulating phase). Lower panel: calculated dc conductivities of each phase. The dotted curve is the fitting function of the form $\sigma_m(T) = 16.8 + 0.01T^{1.5}$. The calculated minimum metallic conductivity (closed square) is also shown.

Thus, from (4) and (7) and knowing the volume fraction, $f_m(T)$, one may calculate the dc conductivity of the Anderson metallic phase, $\sigma_m(0, T)$, as a function of temperature. We found $\sigma_m(0, T)$ exhibits a power-law behaviour $\sigma_m(0, T) = \sigma_0 + bT^{\gamma}$ with $\gamma \approx 1.5 \pm 0.5$, $b \approx 0.01$ and $\sigma_0 \approx 16.8\ \Omega^{-1}\ \mathrm{cm}^{-1}$. The value of σ_0 is in good agreement with the minimum metallic conductivity, $\sigma_0 \approx 0.03e^2/\hbar\xi \approx 13.5\ \Omega^{-1}\ \mathrm{cm}^{-1}$, estimated from the localization length $\xi \approx 60$ Å calculated from the crossover frequency $\omega_c \approx 130\ \mathrm{cm}^{-1}$ [13]. The power-law behaviour suggests that the inelastic scattering time depends on temperature as $\tau_{inelastic} \propto T^{-p}$ with $p \sim 3$ (Lee and Ramakrishnan [1]).

The results depicted in figure 4 bear significant information about the local dynamics of charge carriers. It clearly shows the reason behind the temperature dependence of σ_{dc} and reconciles the differences in the temperature dependence of σ_{dc} and χ data shown in figure 1. Moreover, one may clearly see the physical origin of the levelling off in the temperature dependence of σ_{dc} for temperatures below 60 K; it is due to the combinatorial effect expressed in equation (7). The combination of σ_m, which slowly varies with temperature, and σ_i, which is weakly temperature dependent, together with their slowly changing respective volume fractions gives rise to such complex temperature dependences. In fact, one can reconstruct the measured σ_{dc} by combining the information displayed in the upper and lower panel of figure 4. We could not identify the functional form of σ_i due to the

lack of information below 10 K. However, we anticipate three-dimensional variable-range hopping behaviour.

The issue of the ubiquitous long-range Coulomb interaction among localized carriers is of particular interest. The long-range repulsive Coulomb interaction is expected to modify several physically measurable parameters. First, this interaction would cause $\ln[\sigma_i(0, T)]$ to show a $T^{-1/2}$ temperature dependence rather than a $T^{-1/4}$ dependence characteristic of three-dimensional variable-range hopping of the localized carriers [2, 3]. Second, it is expected to modify the magnetic susceptibility from a Curie dependence, $\chi \approx 1/T$ to a power law behaviour $\chi \approx T^{-\alpha}$ ($\alpha < 1$) according to the electron glass model [14]. Also it has been predicted that the far-infrared conductivity takes the form $\sigma_i(\omega) \approx C_i'\omega/\ln(\omega_0/\omega)$ ($\omega_0 =$ phonon frequency) [15]. Hence, a linear ω dependence of σ_i is expected in the far-infrared range when $\omega \ll \omega_0$ because $\ln(\omega_0/\omega)$ varies slowly with ω.

Because of uncertainties in the data in the analysis described above, we could not determine whether $\ln[\sigma_i(0, T)]$ could be better fitted by a $T^{-1/2}$ or a $T^{-1/4}$ dependence (see figure 5). We find that a reasonable fit to the data for the magnetic susceptibility can be obtained using the power law $\chi \approx T^{-\alpha}$ with $\alpha \approx 0.2$ (see figure 5), as predicted by the

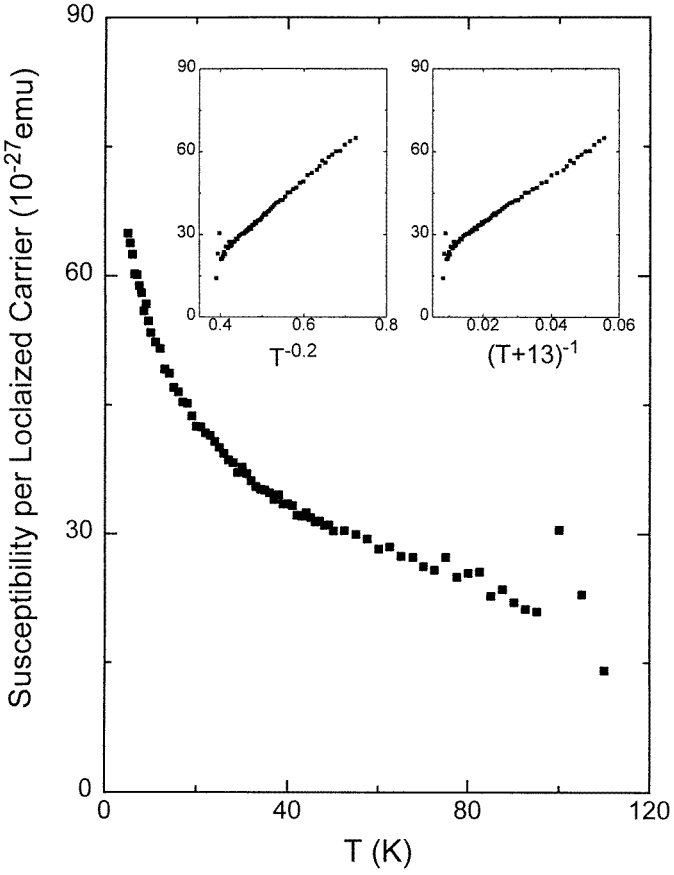

Figure 5. Magnetic susceptibility per localized carrier. The insets show detailed fittings of the susceptibility using a functional from $(T + 13)^{-1}$ and $T^{-0.2}$ (see the text).

electron glass model. However a somewhat better fit is obtained using the form $1/(T+\theta)$ with $\theta = 13$ K, as is also shown in figure 5. The absence of Curie behaviour suggests that there exist Coulomb interactions between localized carriers, although the possible antiferromagnetic behaviour suggests that these interactions may not be fully developed in this temperature range.

However, the manifestation of the Coulomb interaction is ambiguous in the far-infrared conductivity, the tail of which could be fitted by using either the form $\sigma_i(\omega) \approx \omega^{1.0}$ or $\sigma_i(\omega) \approx \omega^{2.0}$. Nonetheless the fit using the form $\sigma_i(\omega) \approx \omega^{1.0}$ failed for frequencies above 80 cm^{-1}. Therefore, it appears that the effect of the Coulomb interaction may be discernible only at very low frequencies. Indeed the Coulomb gap in Si:B was observed only for temperatures below 1.2 K [16] and the linear frequency dependence of $\sigma_i(\omega)$ was confirmed in radio frequency ranges for the temperature span 10 mK $< T <$ 100 mK [17].

Based on the experimental results obtained in this work, the metal–insulator transition in heavily doped silicon may be summarized in the phase diagram depicted in figure 6. At finite temperatures, a genuine metallic state, as defined by Drude-like conductivity and Pauli-like magnetic susceptibility, exists at high temperatures via thermal excitation in a heavily doped semiconductor with $n < n_c$. We propose that the critical carrier density for the metal–insulator transition is a function of temperature. The unusual temperature dependence of σ_{dc} can be explained by the coexistence of two different phases in the system with a temperature-dependent volume fraction of each phase. The Drude and Anderson metallic phases coexist for $T > 110$ K and the insulating and Anderson metallic phases coexist for $T < 110$ K. The thermally induced metal–insulator transition does not show a sharp phase transition boundary because of this coexistence, and the temperature dependence of the relative volume fractions.

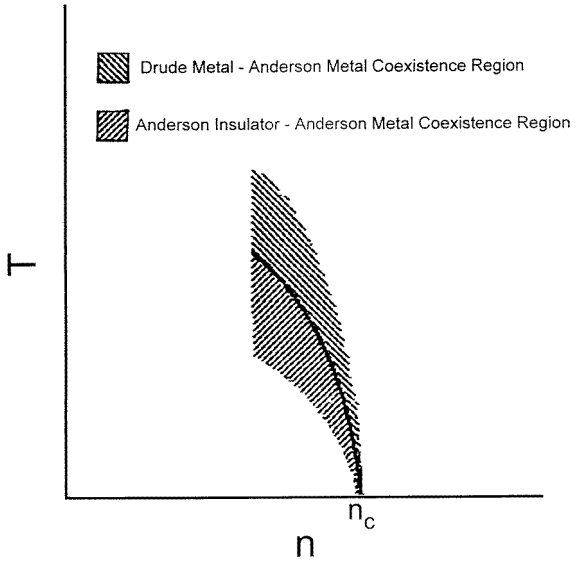

Figure 6. Metal–insulator phase diagram of Si:B.

A further conclusion about the nature of the insulating state can be drawn from this work. Because less than 1% of the carriers go to hydrogen-like bound states with the dopant ions, the insulating state is induced by the random potential. Furthermore ω_c, which

is a measure of the carrier density in the insulating phase, is found to be temperature independent, which confirms our conclusion that the insulating phase does not arise from conversion into hydrogen-like states as temperature is decreased.

References

[1] See for a review, Mott N F 1967 *Adv. Phys.* **16** 49 and
Lee P A and Ramakrishnan T V 1985 *Rev. Mod. Phys.* **57** 287 and references therein
[2] Efros A L and Shklovski B I 1975 *J. Phys. C: Solid State Phys.* **8** L49
Pollak M 1992 *Phil. Mag.* B **65** 657
Altshuler B L and Aronov A G 1979 *Solid State Commun.* **30** 115
[3] Long A P and Pepper M 1984 *J. Phys. C: Solid State Phys.* **17** L425
Shafarman W N, Koon D W and Kastner T G 1989 *Phys. Rev.* B **40** 1216
[4] Pollak M and Geballe T H 1961 *Phys. Rev.* **122** 1742
Serota R A, Yu J and Kim Y H 1993 *Phys. Rev.* B **42** 9724
[5] Dai P, Zhang Y and Sarachik M P 1992 *Phys. Rev.* B **45** 3984
Edwards P P and Sienko M J 1978 *Phys. Rev.* B **17** 2575
[6] Yamanouchi C, Mizuguchi K and Sasaki W 1967 *J. Phys. Soc. Japan* **22** 859
[7] van der Pauw L J 1961 *Phillips Res. Rep.* **16** 187
Montgomery H C 1971 *J. Appl. Phys.* **42** 2971
[8] Altshuller B L, Aronov A G and Khmel'nitskii D E 1981 *Solid State Commun.* **39** 619
Altshuller B L, Aronov A G and Khmel'nitskii D E 1982 *J. Phys. C: Solid State Phys.* **15** 7367
[9] Capizzi M, Thomas G A, DeRosa F, Bhatt R N and Rice T M 1980 *Phys. Rev. Lett.* **44** 1019
Hess H F, DeConde K, Rosenbaum T F and Thomas G A 1992 *Phys. Rev.* B **25** 5578
[10] Thomas G A, Capizzi M, Derosa F, Bhatt R N and Rice T M 1981 *Phys. Rev.* B **23** 5472
[11] Vollhardt D and Wölfle P 1982 *Phys. Rev. Lett.* **48** 699
Shapiro B 1982 *Phys. Rev.* B **25** 4266
Shapiro B and Abrahams E 1981 *Phys. Rev.* B **24** 4889
[12] Li S S 1979 *National Bureau of Standard Publication* 400–47
[13] Mott N F 1981 *Phil. Mag.* B **44** 265
[14] Davis J H, Lee P A and Rice T M 1984 *Phys. Rev.* B **29** 4260
[15] Bhatt R N and Ramakrishnan T V 1984 *J. Phys. C: Solid State Phys.* **17** L639
[16] Massey J G and Lee M 1995 *Phys. Rev. Lett.* **75** 4266
[17] Paalanen M A, Rosenbaum T F, Thomas G A and Bhatt R N 1983 *Phys. Rev. Lett.* **51** 1896